

CD44-Specific A6 Short Peptide Boosts Targetability and Anticancer Efficacy of Polymersomal Epirubicin to Orthotopic Human Multiple Myeloma

Wenxing Gu, Jingnan An, Hao Meng, Na Yu, Yinan Zhong, Fenghua Meng,* Yang Xu,* Jeroen J. L. M. Cornelissen, and Zhiyuan Zhong*

Chemotherapy is widely used in the clinic though its benefits are controversial owing to low cancer specificity. Nanovehicles capable of selectively transporting drugs to cancer cells have been energetically pursued to remodel cancer treatment. However, no active targeting nanomedicines have succeeded in clinical translation to date, partly due to either modest targetability or complex fabrication. CD44-specific A6 short peptide (KPSSPPEE) functionalized polymersomal epirubicin (A6-PS-EPI), which boosts targetability and anticancer efficacy toward human multiple myeloma (MM) in vivo, is described. A6-PS-EPI encapsulating 11 wt% EPI is small (≈ 55 nm), robust, reduction-responsive, and easy to fabricate. Of note, A6 decoration markedly augments the uptake and anticancer activity of PS-EPI in CD44-overexpressing LP-1 MM cells. A6-PS-EPI displays remarkable targeting ability to orthotopic LP-1 MM, causing depleted bone damage and striking survival benefits compared to nontargeted PS-EPI. Overall, A6-PS-EPI, as a simple and intelligent nanotherapeutic, demonstrates high potential for clinical translation.

Chemotherapy based on toxic compounds that primarily inhibit the fast proliferation of the cancer cells is widely used in the clinics though its benefits are controversial owing to a low cancer-specificity and concomitant treatment-related toxic effects.^[1] Nanovehicles capable of selectively transporting drugs to cancer cells have been energetically pursued to provide effective solutions for this dilemma.^[2] Specific (or active) targeting relies on functionalizing the surface of nanovehicles with ligands that are complementary to the target sites.^[3] However, in spite of promise and progress, no actively targeted nanomedicines have succeeded in clinical translation to date, partly due to modest targetability or complex fabrication.^[4] The balance of simplicity and functionality is a key to the success of targeted nanomedicines.^[2a]


Multiple myeloma (MM) is the second most frequent hematologic malignancy that is characterized by clonal proliferation of malignant plasma cells in the bone marrow microenvironment.^[5] Despite increasingly new methods and agents have been validated,^[6] including immunomodulatory drugs,^[7] proteasome inhibitors,^[8] monoclonal antibodies,^[9] and CAR-T cell therapy,^[10] MM remains incurable for a majority of patients. Liposomal nanomedicines such as Doxil and Oncocort IV are also used for the treatment of MM patients,^[11] though their therapeutic benefits are limited as a result of poor MM selectivity. For effective management of MM, targeted formulations are desired.^[12] Interestingly, hematologic cancers including MM are found overexpressing adhesion molecule CD44.^[13] Various CD44 targeting ligands including hyaluronic acid, aptamer, and anti-CD44 antibody^[14] have shown to enhance anti-MM efficacy in vitro and in vivo.^[9a,13c] However, these ligands are big, which complicates fabrication of nanomedicines.

Here, we report for the first time that CD44-specific A6 short peptide (KPSSPPEE) functionalized polymersomal epirubicin (A6-PS-EPI) boosts targetability and anticancer efficacy toward human MM in vivo (**Scheme 1**). A6 is a urokinase-derived peptide that shows a strong binding to CD44 and thereby effective metastasis inhibition of CD44-overexpressing tumors.^[15] Notably, phase I and II human clinical trials displayed that

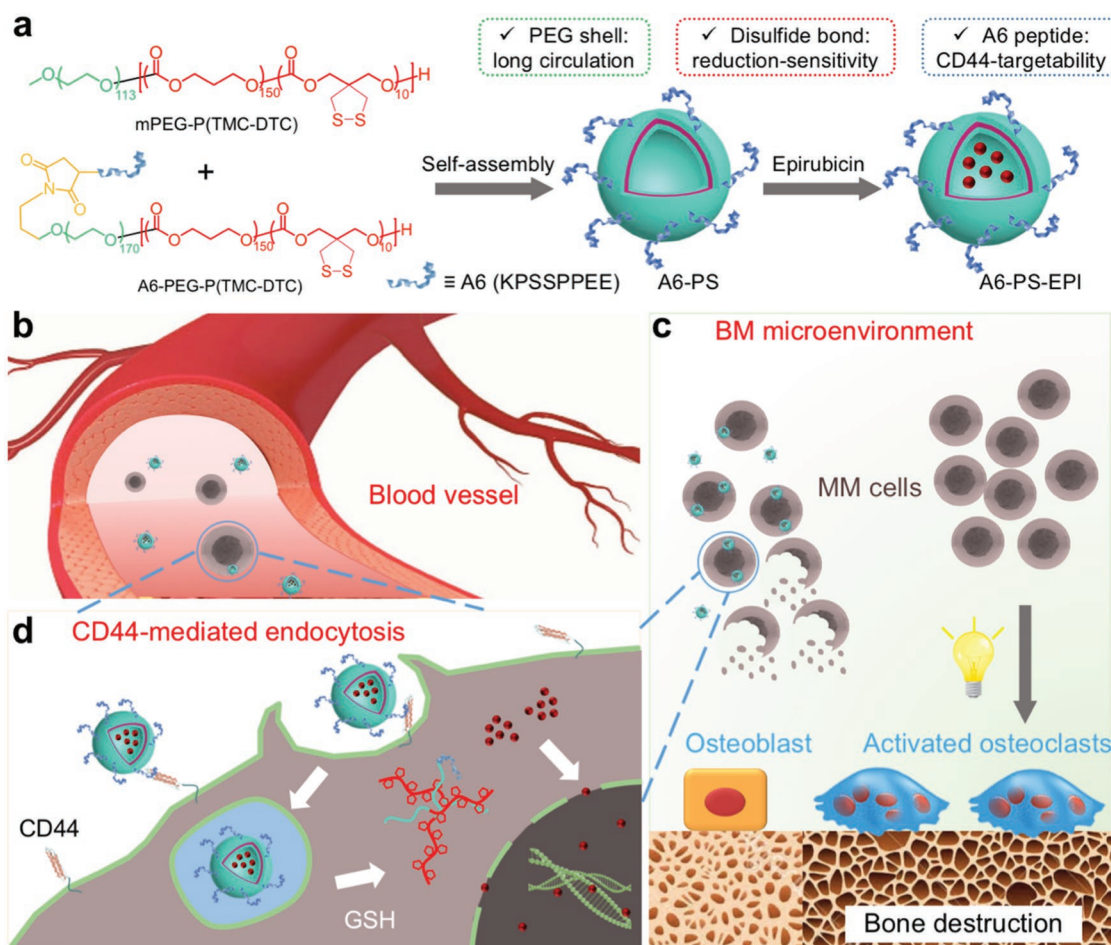
W. X. Gu, H. Meng, N. Yu, Dr. Y. N. Zhong, Prof. F. H. Meng, Prof. Z. Y. Zhong
Biomedical Polymers Laboratory
College of Chemistry
Chemical Engineering and Materials Science
State Key Laboratory of Radiation Medicine and Protection
Soochow University
Suzhou 215123, P. R. China
E-mail: fhmeng@suda.edu.cn; zyzhong@suda.edu.cn

W. X. Gu, Prof. J. J. L. M. Cornelissen
Department of Biomolecular Nanotechnology
MESA+ Institute for Nanotechnology
University of Twente
7500 AE Enschede, The Netherlands

Dr. J. N. An, Prof. Y. Xu
Jiangsu Institute of Hematology
The First Affiliated Hospital of Soochow University
Institute of Blood and Marrow Transplantation of Soochow University
Collaborative Innovation Center of Hematology
Soochow University
Suzhou 215123, P. R. China
E-mail: yangxu@suda.edu.cn

 The ORCID identification number(s) for the author(s) of this article can be found under <https://doi.org/10.1002/adma.201904742>.

DOI: 10.1002/adma.201904742



Scheme 1. Schematic illustration of a) construction and c,d) targeted delivery of CD44-specific A6-PS-EPI in orthotopic LP-1 MM tumor model in vivo. a) A6-PS-EPI is obtained by co-self-assembly of A6-PEG-P(TMC-DTC) and mPEG-P(TMC-DTC) block copolymers followed by loading with epirubicin hydrochloride via pH-gradient method. A6-PS-EPI can actively target to CD44-overexpressing b) MM cells in the circulation as well as c) MM cells homing to bone marrow. d) A6-PS-EPI can be efficiently internalized into MM cells by CD44-mediated uptake and EPI release is accelerated by GSH in the cytosol, leading to selective and potent anti-MM effect.

A6 peptide administered subcutaneously at a high dose of 150–300 mg kg⁻¹ and twice daily has an exceptional safety profile.^[16] Unlike other CD44 targeting ligands, A6 peptide is short, greatly facilitating bio-conjugation and characterization. We have recently developed a robust and reduction-sensitive polymersomal system based on our proprietary dithiolane trimethylene carbonate (DTC) technology that has improved the delivery of various drugs including doxorubicin, siRNA, and protein in different solid tumor models in vivo.^[17] Notably, to maintain the biodegradability of poly(trimethylene carbonate) (PTMC), we introduced only minor amount (about 10 mol%) of DTC, which also shares essentially the same carbonate backbone as TMC, to the polycarbonate block. Epirubicin (EPI) is a widely used drug that exhibits similar anticancer potency while lower cardiotoxicity as compared to doxorubicin. Strikingly, our results show that A6-PS-EPI actively targeted xenografted LP-1 MM cells in vivo, leading to high anti-MM potency and low systemic toxicity. LP-1 MM-bearing mice treated with A6-PS-EPI at 4 mg EPI equiv. kg⁻¹ displayed markedly improved survival rate over the nontargeted PS-EPI and phosphate-buffered saline (PBS) controls (median survival time: 240 days vs 72 and

53 days). Escalating dose to 8 mg EPI equiv. kg⁻¹ further prolonged median survival time to 302 days.

A6-PS-EPI was obtained from co-assembly of mPEG-P(TMC-DTC) and A6-PEG-P(TMC-DTC), which were synthesized with controlled molecular weights (Table S1, Supporting Information) similar as previously reported,^[18] followed by loading of EPI into the watery core by a pH-gradient method (Figure S1, Supporting Information). Free EPI was removed using Sephadex G25 column. The surface density of A6 peptide was tailored by adjusting A6-PEG-P(TMC-DTC) and mPEG-P(TMC-DTC) molar ratios from 10/90, 20/80 to 30/70. As A6-PEG-P(TMC-DTC) has longer polyethylene glycol (PEG) than mPEG-P(TMC-DTC), A6 peptide would likely stretch out and allow effective binding to its receptor, thereby enabling efficient uptake.^[19] A6-PS displayed a high loading of EPI, with drug loading content achieving ≈ 11 wt%. A6-PS-EPI exhibited a small size of ≈ 55 nm and was stable against 10% serum in phosphate buffer (PB, pH 7.4, 10×10^{-3} M) at 37 °C in 24 h, as shown by dynamic laser scattering (DLS; Figure 1a). Remarkably, stability tests corroborated that A6-PS-EPI was stable over 12 months storage in PB at 4 °C (drug leakage less than

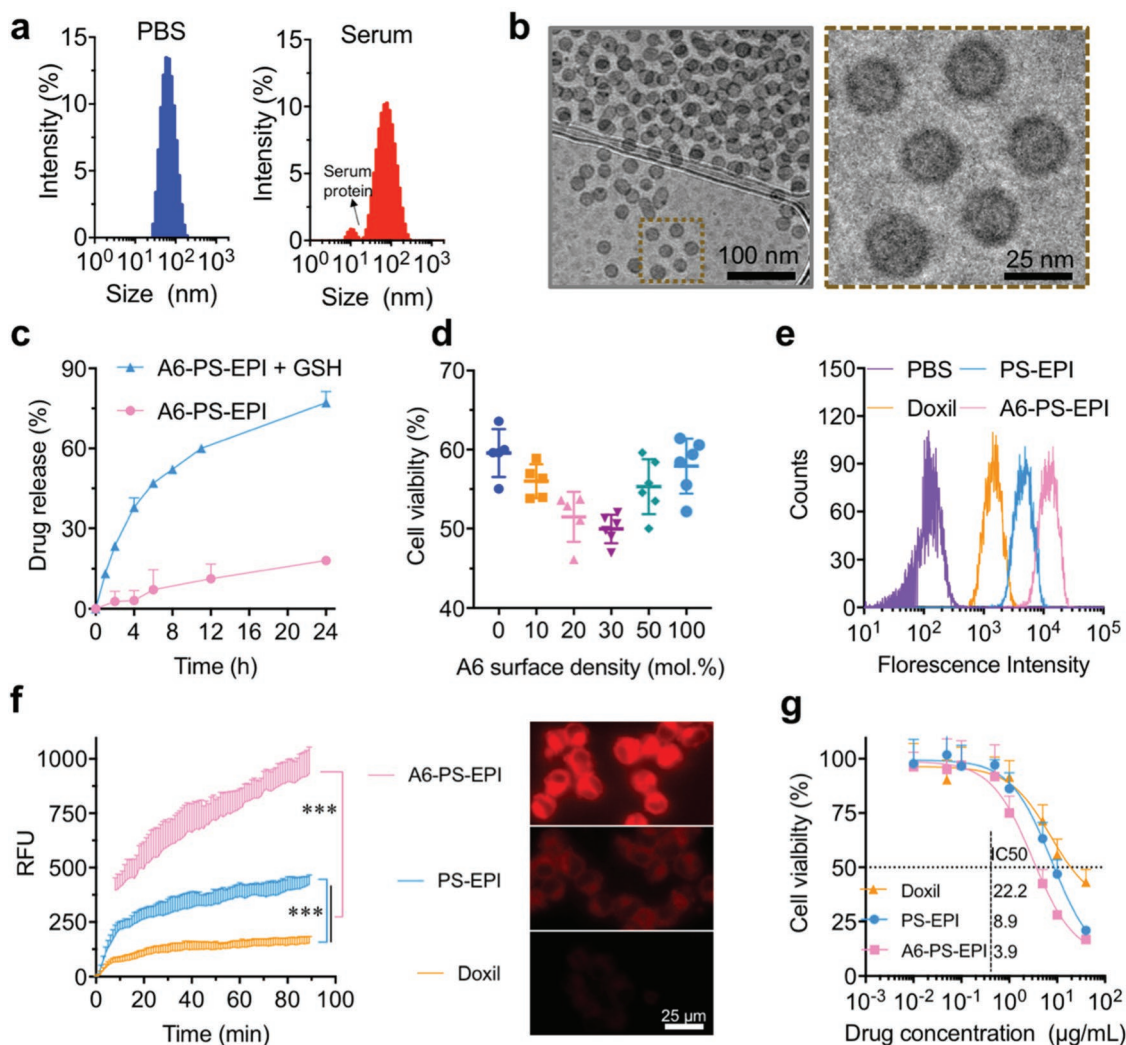


Figure 1. a) Size distribution of A6-PS-EPI in PBS and serum measured by DLS. b) Cryogenic transmission electron micrographs of blank A6-PS-EPI. c) Kinetics of drug release from A6-PS-EPI with or without GSH (10×10^{-3} M). The data are presented as mean \pm standard deviation (SD) ($n = 3$). d) CCK 8 assays of LP-1 cells treated with A6-PS-EPI with varying A6 molar densities ($1 \mu\text{g}$ EPI equiv. mL^{-1}). The cells following 4 h treatment with A6-PS-EPI were cultured in drug-free medium for 44 h. The data are presented as mean \pm SD ($n = 6$). e) Flow cytometric analyses of LP-1 cells following 4 h incubation with A6-PS-EPI, PS-EPI, and Doxil (dose: $10 \mu\text{g}$ drug equiv. mL^{-1}). f) Time-dependent EPI or DOX mean fluorescence intensity in LP-1 cells treated with A6-PS-EPI, PS-EPI, or Doxil (dose: $10 \mu\text{g}$ drug equiv. mL^{-1}) monitored by live cell imaging system (EPI or DOX fluorescence images recorded at 90 min, scale bar: 25 μm). Student *t*-test, *** $p \leq 0.001$. g) The in vitro antitumor activity of A6-PS-EPI, PS-EPI, and Doxil toward LP-1 cells determined by CCK 8 assays. The cells were treated with drug for 4 h and cultured in drug-free medium for 44 h. The data are presented as mean \pm SD ($n = 6$).

0.4%) (Table S2, Supporting Information). The high stability of A6-PS-EPI stems from the autonomous disulfide crosslinking of the polymersomal membrane, as reported previously for DTC-containing polymersomes.^[18] In contrast, nanomedicines including clinical liposomal doxorubicin formulation (Doxil) are often harassed by inadequate stability.^[2b] Cryogenic transmission electron microscopy confirmed that A6-PS had spherical and vesicular morphology and uniform size distribution (Figure 1b). A6-PS-EPI had a slightly negative surface charge of -7.5 mV (Table S3, Supporting Information). Interestingly, under the same fabrication conditions, A6-PS-DOX was obtained with similar drug loading to A6-PS-EPI. The size of A6-PS-DOX was, however, about 12 nm larger than A6-PS-EPI (Table S3, Supporting Information), possibly due to better

packing of EPI than DOX in the polymersomal core. A6-PS-EPI while possessing a high stability under a nonreductive environment released 78% drug in the presence of 10×10^{-3} M glutathione (GSH) in 24 h (Figure 1c), indicating that drug release from A6-PS-EPI would be triggered inside tumor cells.^[18]

It is reported that many MM cells overexpress CD44 that has been employed as a valuable target for MM therapy.^[20] Here, we examined the expression of CD44 of five different MM cells using PE-labeled anti-CD44 antibody by a flow cytometry. The results showed that three cell lines, i.e., LP-1, NCI-H929, and MM.1S, highly expressed CD44 (Figure S2, Supporting Information). Hereafter, we used LP-1 cells as a model to study the targetability and efficacy of A6-PS-EPI. It has been reported that the ligand density on the nanomedicines plays a critical

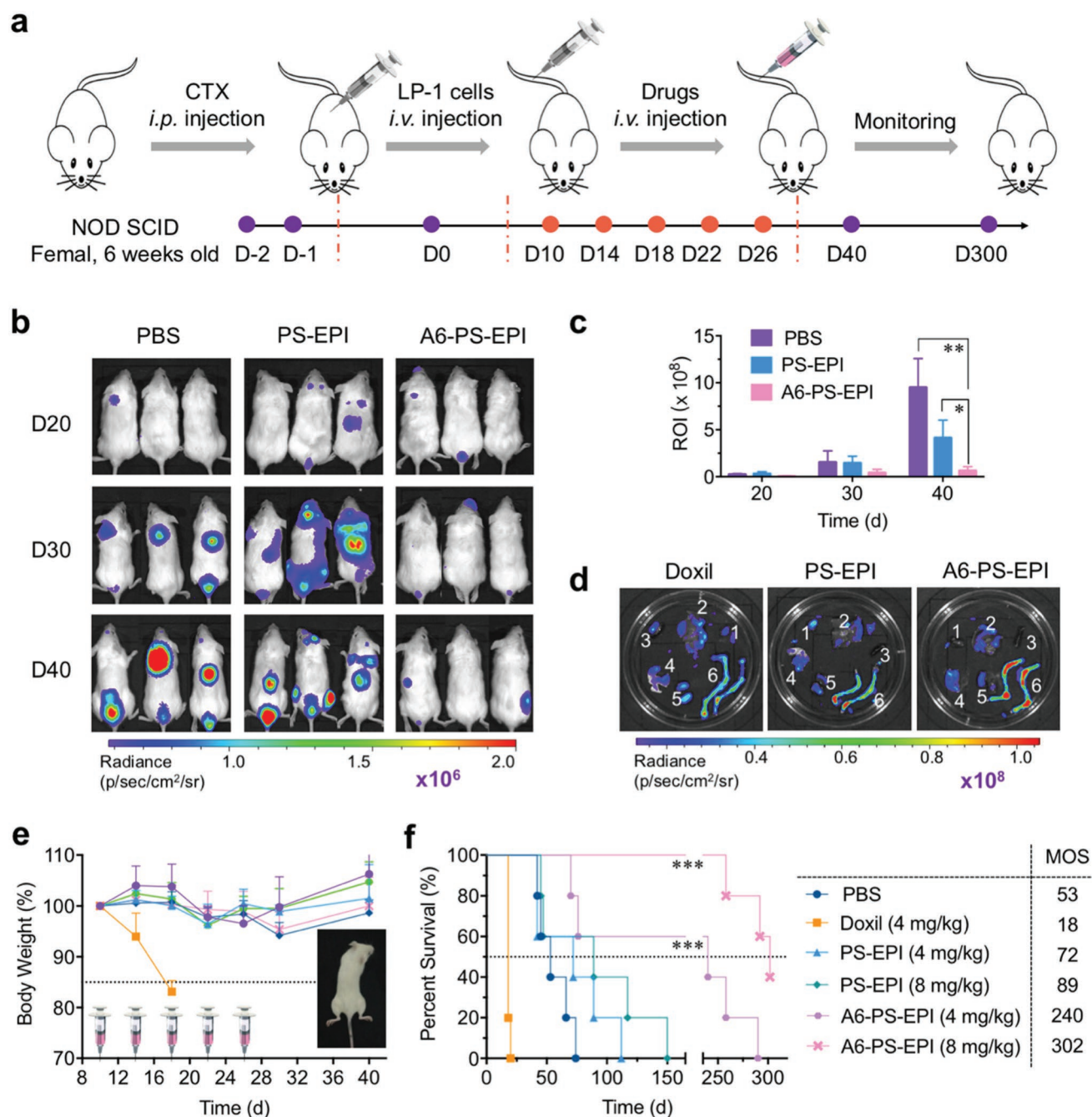


Figure 2. In vivo treatment of A6-PS-EPI, PS-EPI, and Doxil in orthotopic MM model in mice. a) Workflow for building and treating orthotopic MM model. The drugs were injected on day 10, 14, 18, 22, and 26 (dose: 4 or 8 mg drug equiv. kg^{-1} , in 0.2 mL PBS) after implanting MM cells (8 million cells per mouse). b) Images and c) quantitative analysis of in vivo bioluminescence of tumor-bearing mice treated with PBS, PS-EPI, or A6-PS-EPI at different time points (day 20, 30, and 40) after implanting LP-1-luc cells. One-way analysis of variance (ANOVA) with Tukey multiple comparisons tests: $*p \leq 0.05$, $**p \leq 0.01$. d) Ex vivo fluorescence images of the major organs and hind limbs excised at 8 h post-injection of A6-PS-EPI, PS-EPI, or Doxil (dose: 4 mg drug equiv. kg^{-1}) from MM-bearing mice (without treatment) on day 40 after implanting LP-1 cells. 1: heart, 2: liver, 3: spleen, 4: lung, 5: kidney, 6: hind limbs. e) Body weight changes of mice during treatment period. The data are presented as mean \pm SD ($n = 5$). The inset is a mouse showing paralyzed hind limbs. f) Kaplan–Meier survival curves of mice in different treatment groups. MST: median survival time. Log-rank (Mantel–Cox) test was used to quantify differences ($***p \leq 0.001$). The mice were announced death, in case of paralysis of the hind limbs or when the mice became moribund.

role in their targeting ability.^[21] The influence of A6 densities on performance of A6-PS-EPI was first studied. Interestingly, Figure 1d shows that with increasing A6 densities, the anti-tumor efficacy of A6-PS-EPI first increased and then decreased,

with the best killing of LP-1 cells at 30 mol% A6 peptide. If not otherwise specified, A6-PS-EPI referred to the one with 30 mol% A6 peptide. Flow cytometric analyses showed that A6-PS-EPI was 2.4- and 8.6-fold more efficiently internalized

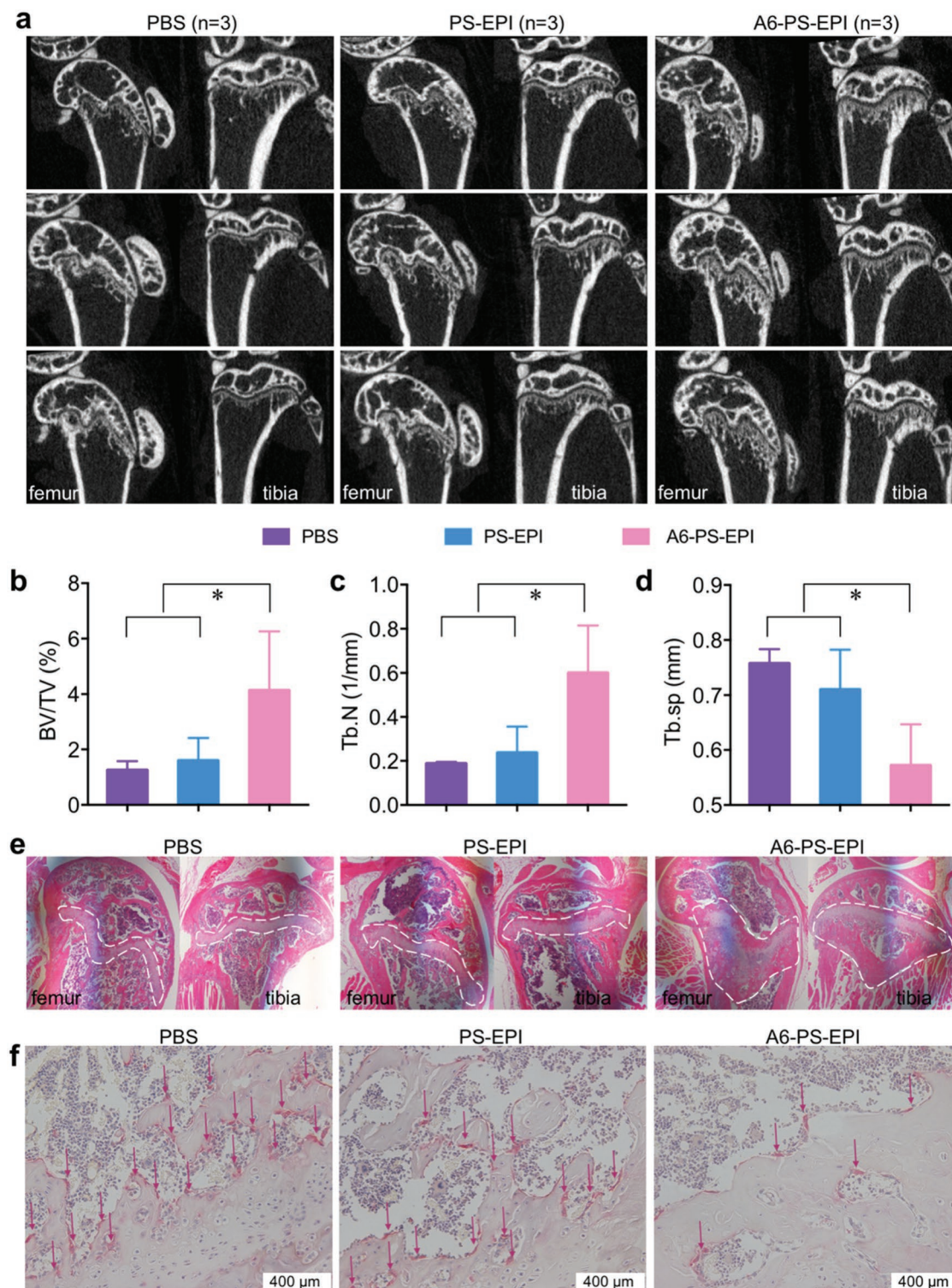


Figure 3. Micro-CT and histological analyses of hind limbs of tumor-bearing mice after treatment with A6-PS-EPI, PS-EPI, or PBS on day 40 ($n = 3$). a) Micro-CT images of cross and longitudinal sections of femurs and tibias. b–d) Quantitative analyses of bone volume fraction (BV/TV), trabecular spacing (Tb.sp), and trabecular bone numbers (Tb.N), respectively. One-way ANOVA with Tukey multiple comparisons tests: $*p \leq 0.05$. e) Histological analysis of hind limbs using H&E staining. The white dashed circles denote the trabecula tissues. f) TRAP staining of osteoclasts (red arrows) in hind limbs. Scale bar: 400 μ m.

by LP-1 cells than nontargeted PS-EPI and Doxil, respectively (Figure 1e). Live cell imaging analyses further displayed significantly faster cell uptake and higher cytoplasmic drug

fluorescence for A6-PS-EPI as compared to PS-EPI and Doxil (Figure 1f). Cell Counting Kit-8 (CCK 8) assays revealed that A6-PS-EPI had a half-maximal inhibitory concentration (IC_{50})

of $3.9 \mu\text{g mL}^{-1}$, which was ≈ 2.3 - and 5.7 -fold lower than PS-EPI and Doxil, respectively (Figure 1g). It is evident that A6-PS-EPI can actively target MM cells and outperforms clinically used Doxil.

To study the performance of A6-PS-EPI *in vivo*, orthotopic MM model was established using NOD/SCID (nonobese diabetic/severe combined immunodeficiency) mice by intravenous (i.v.) injection of LP-1 or LP-1-luc cells. The mice were treated on day 10 post-implantation by i.v. administrating A6-PS-EPI, PS-EPI, or PBS per 4 days for a total of five doses (Figure 2a). The progression of LP-1-Luc was visualized by bioluminescence imaging over time. It is typical that MM tumor cells are disseminated to various sites within the mice.^[22] MM originates in the lymph nodes and accumulates in the bone marrow during disease evolution.^[23] Figure 2b shows that the bioluminescence augmented rapidly from day 10 to 40 in PBS and PS-EPI groups, indicating fast tumor progression. In contrast, low bioluminescence was observed for A6-PS-EPI group in the same period, suggesting effective suppression of LP-1-Luc cell outgrowth. The quantitative bioluminescence analysis (Figure 2c) verified that A6-PS-EPI significantly inhibited MM progression. Interestingly, the *ex vivo* fluorescence images of the organs excised from mice at 8 h post i.v. injection revealed much stronger drug fluorescence in the hind limbs for A6-PS-EPI group compared with PS-EPI or Doxil groups (Figure 2d and Figure S3, Supporting Information), demonstrating improved targetability and accumulation of A6-PS-EPI in the bone that is the main homing site of MM cells. The *in vivo* pharmacokinetic studies showed that A6-PS-EPI had a long circulation time with an elimination half-life of 5.1 h (Figure S4, Supporting Information).

Figure 2e displays that Doxil at $4 \text{ mg DOX equiv. kg}^{-1}$ induced obvious body weight loss and death of mice after the second dose, as a result of low specificity and toxic effects. In sharp contrast, little body weight was lost for A6-PS-EPI and PS-EPI groups, at either 4 or $8 \text{ mg EPI equiv. kg}^{-1}$, supporting the superior safety of A6-PS-EPI and PS-EPI. Notably, PBS group, though kept constant body weight, consecutively exhibited hind-leg paralysis (Figure 2e, the inset), which is a typical symptom of MM progression. Strikingly, LP-1 MM-bearing mice treated with A6-PS-EPI at $4 \text{ mg EPI equiv. kg}^{-1}$ displayed significantly improved survival rate over the nontargeted PS-EPI at the same dosage and PBS controls (median survival time: 240 days vs 72 and 53 days) (Figure 2f). Escalating dose of A6-PS-EPI to $8 \text{ mg EPI equiv. kg}^{-1}$ further prolonged median survival time to 302 days, which was 3.4 - and 5.7 -fold longer than the nontargeted PS-EPI at $8 \text{ mg EPI equiv. kg}^{-1}$ (89 days) and PBS groups, respectively. It is evident that A6-PS-EPI has excellent MM-targeting ability and leads to remarkable survival benefits, which are superior to previously reported nanotherapeutics.^[12,24] For example, anti-CD38 monoclonal antibodies^[25] and very late antigen-4 peptides^[26] guided nanoparticles were reported to improve the therapeutic index of bortezomib and carfilzomib, respectively, but induced only moderate survival benefits. The extraordinary anti-MM potency of A6-PS-EPI is most likely related to its excellent stability, superior selectivity, and accelerated intracellular drug release.

We further examined MM-associated bone damages in mice using micro-CT, hematoxylin & eosin (H&E), and

tartrate-resistant acid phosphatase (TRAP) staining techniques. Figure 3a and Figure S5 in the Supporting Information show that A6-PS-EPI group had obviously less osteolytic lesions in the hind limb bones than PS-EPI and PBS groups. Quantitative analyses (Figure 3b–d and Figure S6, Supporting Information) revealed that A6-PS-EPI group had significantly higher bone volume fraction and trabecular number while significantly lower bone surface fraction and trabecular spacing than PS-EPI and PBS groups, indicating effective prevention of MM-associated osteolytic lesions by A6-PS-EPI treatment. Moreover, histological analyses (Figure 3e) confirmed that A6-PS-EPI group had clear bone trabecula structure and less osteolytic lesions which are usually caused by tumor infiltration. MM-associated bone damage is generally considered owing to the imbalance between osteoblasts and osteoclasts, in which osteoclast activity increases due to an enhanced production of receptor activator of nuclear factor kappa ligand by MM cells and reduced production of osteoprotegerin by osteoblasts or bone marrow stromal cells.^[27] TRAP staining was performed to gauge the activity of osteoclasts in femurs and tibias. Notably, TRAP staining exhibited that A6-PS-EPI group had obviously less activity of osteoclasts than control groups (Figure 3f), supporting that bone damage in MM xenografts is associated with the activation of osteoclasts and A6-PS-EPI can effectively suppress osteoclast activation. Furthermore, H&E staining revealed that A6-PS-EPI induced little damage of major organs (Figure S7, Supporting Information), supporting that A6-PS-EPI has low systemic toxicity.

In summary, we have demonstrated that CD44-specific A6 short peptide-functionalized polymersomal epirubicin (A6-PS-EPI) holds extraordinary targetability and anticancer performance toward orthotopic human MM xenografts *in vivo*, causing depleted bone damage and striking survival benefits compared to nontargeted PS-EPI as well as clinically used Doxil. Interestingly, A6-PS-EPI, while possessing desired merits including small size, high drug loading, excellent stability, good safety, CD44 specificity, and bio-responsivity, has remarkable simplicity in formulation, lending it a high potential for clinical translation. Unlike liposomes that need to be PEGylated to obtain stealthy formulation, A6-PS-EPI with an intrinsic and dense layer of PEG shell is better stealthed and more stable over storage and in circulation. Inadequate stability is a big problem for liposomal formulations including Doxil. Given their low stability, it is practically challenging to develop actively targeted formulations based on liposomes. This is a first report on CD44-specific short peptide for highly efficient and actively targeted chemotherapy of MM, which may further extend to targeted treatment of different CD44 positive hematologic malignancies and solid tumors.

Supporting Information

Supporting Information is available from the Wiley Online Library or from the author.

Acknowledgements

W.G. and J.A. contributed equally to this work. This work was supported by research grants from the National Natural Science Foundation

of China (NSFC 51633005, 51773146, 51861145310, 51561135010, 51761135117) and a Project Funded by the Priority Academic Program Development (PAPD) of Jiangsu Higher Education Institutions. All animal experiments were approved by the Animal Care and Use Committee of Soochow University (P. R. China), and all protocols of animal studies conformed to the Guide for the Care and Use of Laboratory Animals.

Conflict of Interest

The authors declare no conflict of interest.

Keywords

chemotherapy, multiple myelomas, nanomedicine, polymersomes, targeted delivery

Received: July 24, 2019

Revised: September 11, 2019

Published online: September 27, 2019

- [1] a) J. Wolfram, M. Ferrari, *Nano Today* **2019**, 25, 85; b) M. E. Davis, Z. G. Chen, D. M. Shin, *Nat. Rev. Drug Discovery* **2008**, 7, 771.
- [2] a) D. Rosenblum, N. Joshi, W. Tao, J. M. Karp, D. Peer, *Nat. Commun.* **2018**, 9, 1410; b) J. Shi, P. W. Kantoff, R. Wooster, O. C. Farokhzad, *Nat. Rev. Cancer* **2017**, 17, 20.
- [3] a) S. Wilhelm, A. J. Tavares, Q. Dai, S. Ohta, J. Audet, H. F. Dvorak, W. C. W. Chan, *Nat. Rev. Mater.* **2016**, 1, 16014; b) H. Sun, Y. Dong, J. Feijen, Z. Zhong, *J. Controlled Release* **2018**, 290, 11; c) P. Zhang, L. Zhang, Z. Qin, S. Hua, Z. Guo, C. Chu, H. Lin, Y. Zhang, W. Li, X. Zhang, X. Chen, G. Liu, *Adv. Mater.* **2018**, 30, 1705350.
- [4] a) Q. Sun, Z. Zhou, N. Qiu, Y. Shen, *Adv. Mater.* **2017**, 29, 1606628; b) Y. Min, J. M. Caster, M. J. Eblan, A. Z. Wang, *Chem. Rev.* **2015**, 115, 11147.
- [5] a) A. J. Cowan, C. Allen, A. Barac, H. Basaleem, I. Bensenor, M. P. Curado, K. Foreman, R. Gupta, J. Harvey, H. D. Hosgood, M. Jakovljevic, Y. Khader, S. Linn, D. Lad, L. Mantovani, V. M. Nong, A. Mokdad, M. Naghavi, M. Postma, G. Roshandel, K. Shackelford, M. Sisay, C. T. Nguyen, T. T. Tran, B. T. Xuan, K. N. Ukwaja, S. E. Vollset, E. Weiderpass, E. N. Libby, C. Fitzmaurice, *JAMA Oncol.* **2018**, 4, 1221; b) A. Palumbo, K. Anderson, *N. Engl. J. Med.* **2011**, 364, 1046.
- [6] a) J. Ubels, P. Sonneveld, E. H. van Beers, A. Broijl, M. H. van Vliet, J. de Ridder, *Nat. Commun.* **2018**, 9, 2943; b) S. Manier, J. Park, M. Capelletti, M. Bustoros, S. S. Freeman, G. Ha, J. Rhoades, C. J. Liu, D. Huynh, S. C. Reed, G. Gydush, K. Z. Salem, D. Rotem, C. Freymond, A. Yosef, A. Perilla-Glen, L. Garderet, E. M. Van Allen, S. Kumar, J. C. Love, G. Getz, V. A. Adalsteinsson, I. M. Ghobrial, *Nat. Commun.* **2018**, 9, 1691.
- [7] a) M. Kohler, C. Greil, M. Hudecek, S. Lonial, N. Raje, R. Wasch, M. Engelhardt, *Cancer* **2018**, 124, 2075; b) C. Varga, J. P. Laubach, K. C. Anderson, P. G. Richardson, *Br. J. Haematol.* **2018**, 181, 433.
- [8] Q. Hu, C. Qian, W. Sun, J. Wang, Z. Chen, H. N. Bomba, H. Xin, Q. Shen, Z. Gu, *Adv. Mater.* **2016**, 28, 9573.
- [9] a) C. Varga, M. Maglio, I. M. Ghobrial, P. G. Richardson, *Br. J. Haematol.* **2018**, 181, 447; b) M. A. Dimopoulos, D. Dytfield, S. Grosicki, P. Moreau, N. Takezako, M. Hori, X. Leleu, R. LeBlanc, K. Suzuki, M. S. Raab, P. G. Richardson, M. Popa McKiver, Y.-M. Jou, S. G. Shelat, M. Robbins, B. Rafferty, J. San-Miguel, *N. Engl. J. Med.* **2018**, 379, 1811.
- [10] a) N. Hosen, Y. Matsunaga, K. Hasegawa, H. Matsuno, Y. Nakamura, M. Makita, K. Watanabe, M. Yoshida, K. Satoh, S. Morimoto, F. Fujiki, H. Nakajima, J. Nakata, S. Nishida, A. Tsuboi, Y. Oka, M. Manabe, H. Ichihara, Y. Aoyama, A. Mugitani, T. Nakao, M. Hino, R. Uchibori, K. Ozawa, Y. Baba, S. Terakura, N. Wada, E. Morii, J. Nishimura, K. Takeda, Y. Oji, H. Sugiyama, J. Takagi, A. Kumanogoh, *Nat. Med.* **2017**, 23, 1436; b) N. S. Ramadoss, A. D. Schulman, S. H. Choi, D. T. Rodgers, S. A. Kazane, C. H. Kim, B. R. Lawson, T. S. Young, *J. Am. Chem. Soc.* **2015**, 137, 5288.
- [11] A. K. Deshantri, A. Varela Moreira, V. Ecker, S. N. Mandhane, R. M. Schifferers, M. Buchner, M. Fens, *J. Controlled Release* **2018**, 287, 194.
- [12] A. Detappe, M. Bustoros, T. H. Mouhieddine, P. P. Ghoroghchian, *Trends Mol. Med.* **2018**, 24, 560.
- [13] a) F. Birzele, E. Voss, A. Nopora, K. Honold, F. Heil, S. Lohmann, H. Verheul, C. Le Tourneau, J. P. Delord, C. van Herpen, D. Mahalingam, A. L. Coveler, V. Meresse, S. Weigand, V. Runza, M. Cannarile, *Clin. Cancer Res.* **2015**, 21, 2753; b) M. Zoller, *Nat. Rev. Cancer* **2011**, 11, 254; c) C. C. Bjorklund, V. Baladandayuthapani, H. Y. Lin, R. J. Jones, I. Kuitse, H. Wang, J. Yang, J. J. Shah, S. K. Thomas, M. Wang, D. M. Weber, R. Z. Orlowski, *Leukemia* **2014**, 28, 373.
- [14] a) Y. Zhong, J. Zhang, R. Cheng, C. Deng, F. Meng, F. Xie, Z. Zhong, *J. Controlled Release* **2015**, 205, 144; b) L. Arabi, A. Badiie, F. Mosaffa, M. R. Jaafari, *J. Controlled Release* **2015**, 220, 275; c) W. Alshaer, H. Hillaireau, J. Vergnaud, S. Mura, C. Deloménie, F. Sauvage, S. Ismail, E. Fattal, *J. Controlled Release* **2018**, 271, 98.
- [15] a) M. Finlayson, *Front. Immunol.* **2015**, 6, 135; b) R. S. Piotrowicz, B. B. Damaj, M. Hachicha, F. Incardona, S. B. Howell, M. Finlayson, *Mol. Cancer Ther.* **2011**, 10, 2072; c) K. Mishima, A. P. Mazar, A. Gown, M. Skelly, X.-D. Ji, X.-D. Wang, T. R. Jones, W. K. Cavenee, H.-J. S. Huang, *Proc. Natl. Acad. Sci. U. S. A.* **2000**, 97, 8484.
- [16] S. A. Ghamande, M. H. Silverman, W. Huh, K. Behbakht, G. Ball, L. Cuasay, S. O. Würtz, N. Brunner, M. A. Gold, *Gynecol. Oncol.* **2008**, 111, 89.
- [17] a) Y. Jiang, W. Yang, J. Zhang, F. Meng, Z. Zhong, *Adv. Mater.* **2018**, 30, 1800316; b) Y. Zou, M. Zheng, W. Yang, F. Meng, K. Miyata, H. J. Kim, K. Kataoka, Z. Zhong, *Adv. Mater.* **2017**, 29, 1703285; c) Y. Zou, Y. Xia, F. Meng, J. Zhang, Z. Zhong, *Mol. Pharmaceutics* **2018**, 15, 3664.
- [18] Y. Zou, F. Meng, C. Deng, Z. Zhong, *J. Controlled Release* **2016**, 239, 149.
- [19] J. F. Stefanick, J. D. Ashley, T. Kiziltepe, B. Bilgicer, *ACS Nano* **2013**, 7, 2935.
- [20] M. Casucci, B. N. d. Robilant, L. Falcone, B. Camisa, M. Norelli, P. Genovese, B. Gentner, F. Gullotta, M. Ponzone, M. Bernardi, M. Marcati, A. Saudemont, C. Bordonign, B. Savoldo, F. Ciceri, L. Naldini, G. Dotti, C. Bonini, A. Bondanza, *Blood* **2013**, 122, 3461.
- [21] D. Liu, P. Guo, C. McCarthy, B. Wang, Y. Tao, D. Auguste, *Nat. Commun.* **2018**, 9, 2612.
- [22] A. A. Postnov, H. Rozemuller, V. Verwey, H. Lokhorst, N. De Clerck, A. C. Martens, *Calcif. Tissue Int.* **2009**, 85, 434.
- [23] D. Zhu, Z. Wang, J. J. Zhao, T. Calimeri, J. Meng, T. Hideshima, M. Fulciniti, Y. Kang, S. B. Ficarro, Y. T. Tai, Z. Hunter, D. McMillin, H. Tong, C. S. Mitsiades, C. J. Wu, S. P. Treon, D. M. Dorfman, G. Pinkus, N. C. Munshi, P. Tassone, J. A. Marto, K. C. Anderson, R. D. Carrasco, *Nat. Med.* **2015**, 21, 572.
- [24] A. Swami, M. R. Reagan, P. Basto, Y. Mishima, N. Kamaly, S. Glavey, S. Zhang, M. Moschetta, D. Seevaratnam, Y. Zhang, J. Liu, M. Memarzadeh, J. Wu, S. Manier, J. Shi, N. Bertrand, Z. N. Lu, K. Nagano, R. Baron, A. Sacco, A. M. Roccaro, O. C. Farokhzad, I. M. Ghobrial, *Proc. Natl. Acad. Sci. U. S. A.* **2014**, 111, 10287.
- [25] P. de la Puente, M. J. Luderer, C. Federico, A. Jin, R. C. Gilson, C. Egbulefu, K. Alhallak, S. Shah, B. Muz, J. Sun, J. King, D. Kohnen,

- N. N. Salama, S. Achilefu, R. Vij, A. K. Azab, *J. Controlled Release* **2018**, *270*, 158.
- [26] J. D. Ashley, J. F. Stefanick, V. A. Schroeder, M. A. Suckow, N. J. Alves, R. Suzuki, S. Kikuchi, T. Hideshima, K. C. Anderson, T. Kiziltepe, B. Bilgicer, *J. Controlled Release* **2014**, *196*, 113.
- [27] a) S. K. Kumar, V. Rajkumar, R. A. Kyle, M. van Duin, P. Sonneveld, M. V. Mateos, F. Gay, K. C. Anderson, *Nat. Rev. Dis. Primers* **2017**, *3*, 17046; b) N. Raje, G. D. Roodman, *Clin. Cancer Res.* **2011**, *17*, 1278; c) E. Terpos, I. Ntanasis-Stathopoulos, M. Gavriatopoulou, M. A. Dimopoulos, *Blood Cancer J.* **2018**, *8*, 7.